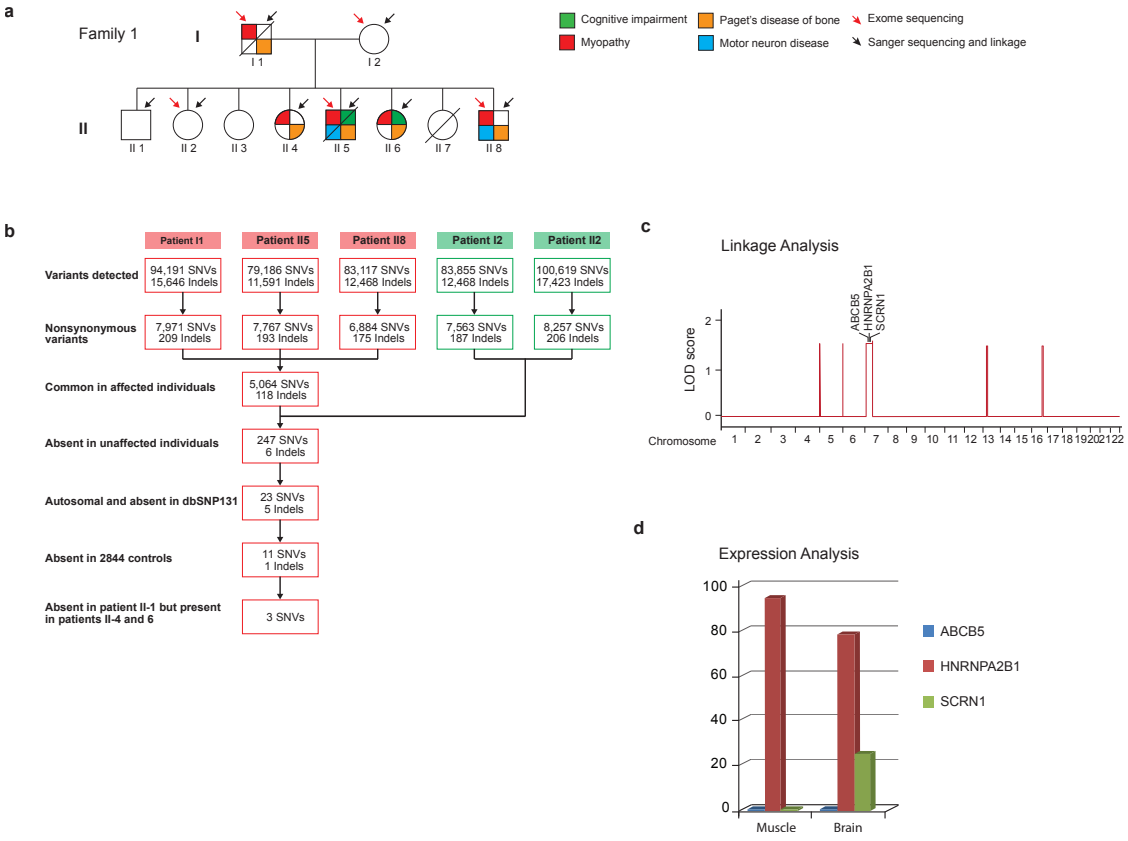

Figure 1. Identification of the disease-causing mutation in family 1. **a.** The pedigree of family 1 indicating individuals affected by cognitive impairment, myopathy, PDB, and motor neuron disease[1]. Patient I1 had behavioral changes, weakness, muscle atrophy, and progressive skeletal abnormalities. At autopsy, he was diagnosed with FTD, IBM, and PDB. The affected children had onset of weakness and skeletal abnormalities in their 20s, which was slowly progressive. Two of the children (patients II5 and II6) showed evidence of impaired executive function upon cognitive exam. Muscle biopsy (patients II4, II5, and II6) showed groups of small atrophic fibers and rimmed vacuoles characteristic of IBM in addition to regions of grouped atrophy. Radiological and serum evaluation (patients II4, II5, II6, and II8) confirmed diagnoses of PDB. Electrophysiological examination (II5 and II8) showed motor neuron dysfunction in addition to myopathic features. Patient II8 subsequently succumbed to rapidly progressive weakness. **b.** The filtering paradigm used to detect novel sequence variants that co-segregated with disease is shown. Affected patients represented by red and unaffected patients by green. **c.** The results of linkage analysis in family 1 is shown and the location of the 3 SNVs that co-segregated with disease is indicated. **d.** The relative expression levels of hnRNPA2/B1, SCRN1, and ABCB5 in muscle and brain are indicated as determined by RNAseq. Not only is there limited to no expression of SCRN11 and ABCB5 in affected tissues, the variants we identified in these genes were subsequently identified by the NHLBI Exome Sequencing Project as polymorphisms present in the normal population (see Table 1).

Gene	Location	Chromosome	Allele Variant (Ref/patient)	Variant Type	Amino Acid Change	Residue Conserved?	Expressed in Adult Muscle and CNS?	Polyphen Prediction	Absent polymorphism in NHLBI Exome Sequencing Project
HNRNPA2B1	26232966	7	A/T	SNV	D290V (isoform A2) D302V (isoform B1)	Yes	Yes	Damaging	Yes
ABCB5	20784996	7	T/G	SNV	L677V	No	No	Benign	No
SCRN1	30008638	7	G/A	SNV	R16C (isoform a) R36C (isoform b)	No	Detectable	Benign	No

Table 1. Summary table of data relating to the 3 SNVs that co-segregate with disease in family 1.

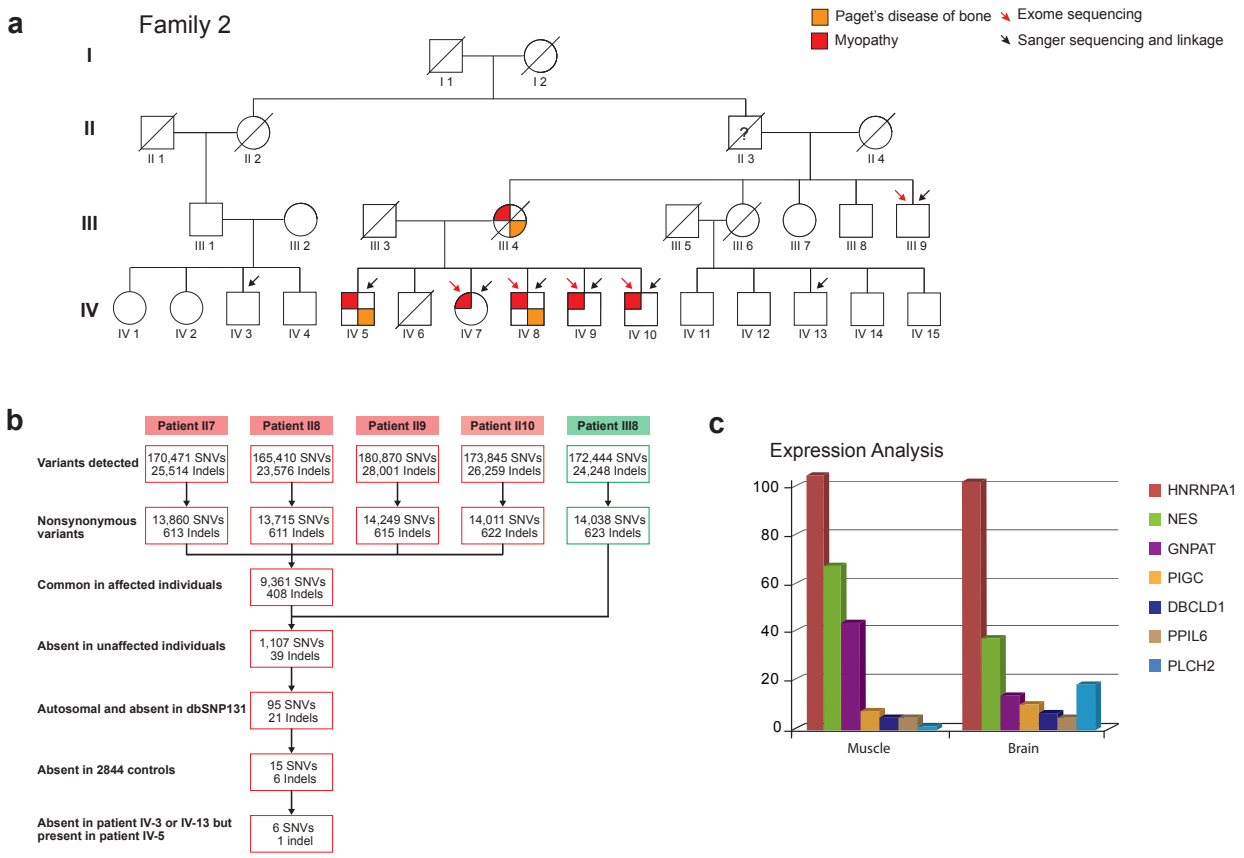

Figure 2. Identification of the disease-causing mutation in family 2. **a.** The full pedigree of family 2 indicating individuals affected by myopathy and PDB. **b.** The filtering paradigm used to detect novel sequence variants that co-segregated with disease is shown. Affected patients represented by red and unaffected patients by green. **c.** The relative expression levels of candidate genes in muscle and brain are indicated as determined by RNAseq. Subsequently, the PPIL6 variant was identified as a polymorphism in the normal population by the NHLBI Exome Sequencing Project (see Table 2).

Gene	Location	Chromosome	Allele Variant (Ref/patient)	Variant Type	Amino Acid Change	Residue Conserved?	Expressed in Adult Muscle and CNS?	Polyphen Prediction	Absent polymorphism in NHLBI Exome Sequencing Project
HNRNPA1	54677629	12	A/T	SNV	D262V (isoform a) D314V (isoform b)	Yes	Yes	Damaging	Yes
NES	156641885	1	G/A	SNV	P699S	No	Yes	Benign	Yes
DCBLD1	117825031	6	G/A	SNV	I72V	No	Detectable	Possibly damaging	Yes
PPIL6	109752445	6	A/G	SNV	V80A (isoform 1) V112A (isoform 2)	No	Detectable	Benign	No
PIGC	172411650	1	C/T	SNV	R38Q	No	Detectable	Benign	Yes
GNPAT	231386768	1	A/C	SNV	D47A	No	Yes	Possibly damaging	Yes
PLCH2	2435831	1	Tcc/---	Deletion	S1144del	N/A	Detectable	N/A	Yes

Table 2. Summary table of data relating to the 6 SNVs and 1 indel that co-segregate with disease in family 2.

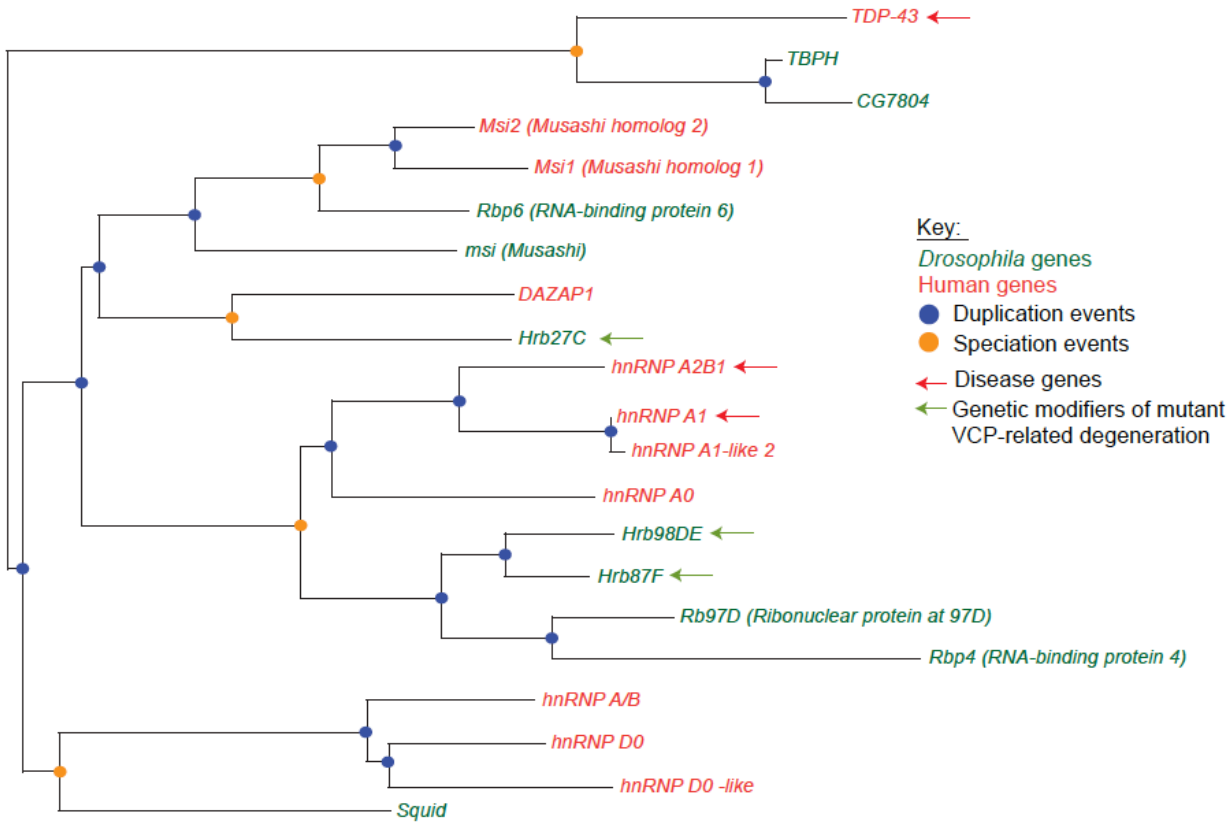

Figure 3. Orthology/paralogy assignment of hnRNP A/B proteins in Drosophila melanogaster and Homo sapiens. Phylogenetic analysis was used to resolve the orthological/paralogical relations among human and drosophila proteins that show homology to TBPH. Twenty-one genes were shown in the phylogram, in which drosophila and human genes are in red and green colors, respectively. The node colors denote duplication events (red nodes) and speciation events (green nodes). Disease genes indicated with red arrow and genetic modifiers of VCP-related degeneration indicated with green arrow[2].

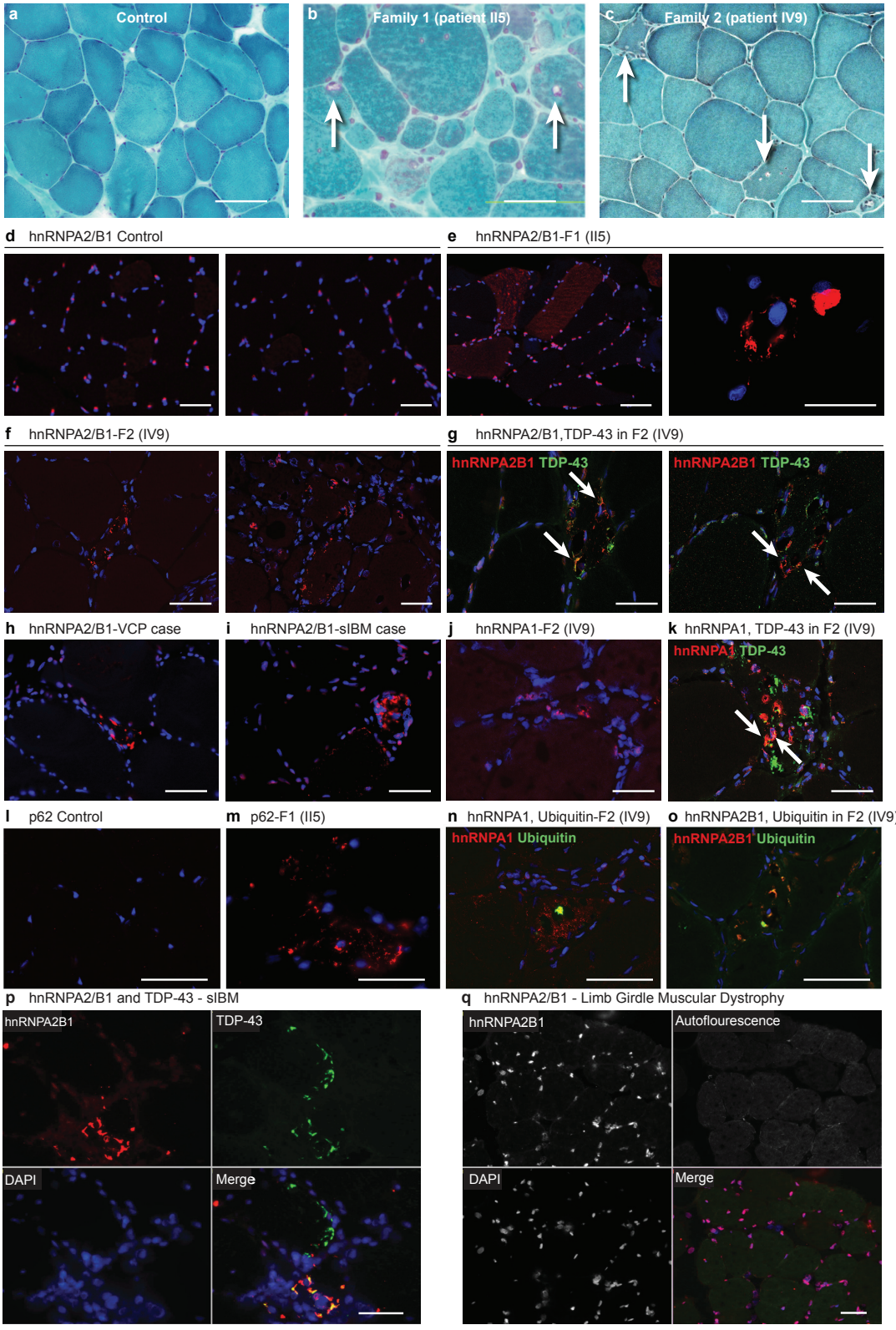
a Control
b Family 1 (patient II5)
c Family 2 (patient IV9)
d hnRNPA2/B1 Control
e hnRNPA2/B1-F1 (II5)
f hnRNPA2/B1-F2 (IV9)
g hnRNPA2/B1,TDP-43 in F2 (IV9)
hnRNPA2B1 TDP-43
hnRNPA2B1 TDP-43
h hnRNPA2/B1-VCP case
i hnRNPA2/B1-sIBM case
j hnRNPA1-F2 (IV9)
k hnRNPA1, TDP-43 in F2 (IV9)
hnRNPA1 TDP-43
l p62 Control
m p62-F1 (II5)
n hnRNPA1, Ubiquitin-F2 (IV9)
o hnRNPA2B1, Ubiquitin in F2 (IV9)
hnRNPA1 Ubiquitin
hnRNPA2B1 Ubiquitin
p hnRNPA2/B1 and TDP-43 - sIBM
hnRNPA2B1
TDP-43
DAPI
Merge
q hnRNPA2/B1 - Limb Girdle Muscular Dystrophy
hnRNPA2B1
Autoflourescence
DAPI
Merge

Figure 4. Nuclear clearance and accumulation of pathological sarcoplasmic inclusions of hnRNPA2/B1 and hnRNPA1 in patients. **a-c.** Gomori trichrome staining in a normal muscle sample (**a**), a muscle biopsy from patient II5 from family 1 (**b**) and patient IV9 from family 2 (**c**). Arrows indicate rimmed vacuoles. **d-f.** Immunohistochemical analysis of hnRNPA2/B1 (red) in a normal muscle sample (**d**), a muscle biopsy from patient II5 from family 1 (**e**), a muscle biopsy from patient IV9 from family 2 (**f**). hnRNPA2/B1 (red) was cleared from DAPI-stained myonuclei (blue) and accumulated in large sarcoplasmic inclusions in patients (**e, f**). **g**. Immunohistochemical analysis of hnRNPA2/B1 and TDP-43 colocalization in a muscle biopsy from patient IV9 from family 2. DAPI (blue), TDP-43 (green), and hnRNPA2/B1 (red) are shown. hnRNPA2/B1 (red) and TDP-43 (green) were partially colocalizing (arrows) in an atropic muscle fiber. **h-i.** Immunohistochemical analysis of hnRNPA2/B1 in a patient with MSP caused by VCP mutation (R155H) (**h**), and a patient with sporadic IBM (**i**). **j.** Immunohistochemical analysis of hnRNPA1 in a muscle biopsy from patient IV9 from family 2. **k.** Immunohistochemical analysis of hnRNPA1 and TDP-43 colocalization in a muscle biopsy from patient IV9 from family 2. DAPI (blue), TDP-43 (green), and hnRNPA1 (red) are shown. hnRNPA1 (red) and TDP-43 (green) were partially colocalizing (arrows) in an atropic muscle fiber. **l-m**. Immunohistochemical analysis of p62 in a normal muscle sample (**l**) and a muscle biopsy from patient II5 from family 1 (**m**). p62 was accumulated in large sarcoplasmic inclusions in patient (**m**). **n-o**. Immunohistochemical analysis of ubiquitin and hnRNPA1 (**n**) and hnRNPA2/B1 (**o**) in a muscle biopsy from patient IV9 from family 2. In both cases, limited immunopositivity of ubiquitin was observed in a large sarcoplasmic inclusions (arrows). **p.** Immunohistochemical analysis of hnRNPA2/B1 and TDP-43 colocalization in a patient with sporadic IBM. hnRNPA2/B1 (red) and TDP-43 (green) were partially colocalizing. **q**. No hnRNPA2/B1 pathology was observed in a patient with limb-girdle muscular dystrophy.

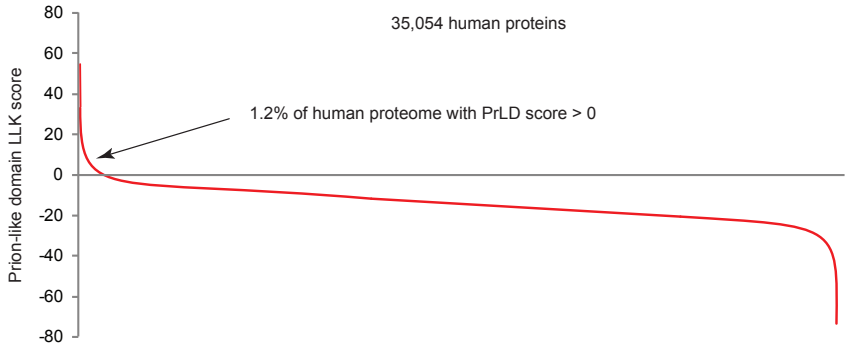

Figure 5. Examination of the human proteome (35,054 RefSeq proteins, including variant isoforms) identified possible PrLDs in approximately 1.2 %, according to the algorithm of Alberti et al. The list of possible PrLD-containing proteins was rich in proteins that regulate RNA metabolism.

Gene Name	PrLD Rank Among All Proteins	PrLD Score	Comment
FUS	13	37.6	ALS, FTD
TAF15	22	33.2	ALS, FTD
EWSR1	25	32.4	ALS, FTD
HNRPDL	28	31.5	
HNRNPD	30	30.6	
HNRNPA2B1	32	29.9	Family 1
HNRNPA1	38	28.2	Family 2
HNRNPAB	39	27.3	
HNRNPA3	41	27.2	
TARDBP	43	26.5	ALS, FTD, IBM
TIA1	55	23.2	
HNRNPA1L2	57	22.8	
HNRNPH1	63	22.3	
AC021224.2	68	21.6	
SFPQ	79	20.8	
HNRNPA0	81	20.6	
HNRNPH2	98	17.5	
RBM14	117	16.1	
CSTF2	122	15.7	
AC021593.2	124	15.4	
DAZ3	136	14.6	
DAZ1	143	14.1	
DAZ2	143	14.1	
DAZ4	143	14.1	
CSTF2T	148	14	
HNRNPH3	147	14	
TIAL1	158	13.5	
RBM33	172	12.9	
CELF4	176	12.8	
DAZAP1	198	11.7	
PSPC1	226	10	

Table 3. Predicted PrLD containing proteins that have an RRM are shown. In addition to hnRNPA2B1 and hnRNPA1, this list included several proteins previously implicated in human degenerative proteinopathies, as indicated. This observation was also made by Couthouis et al.[3]

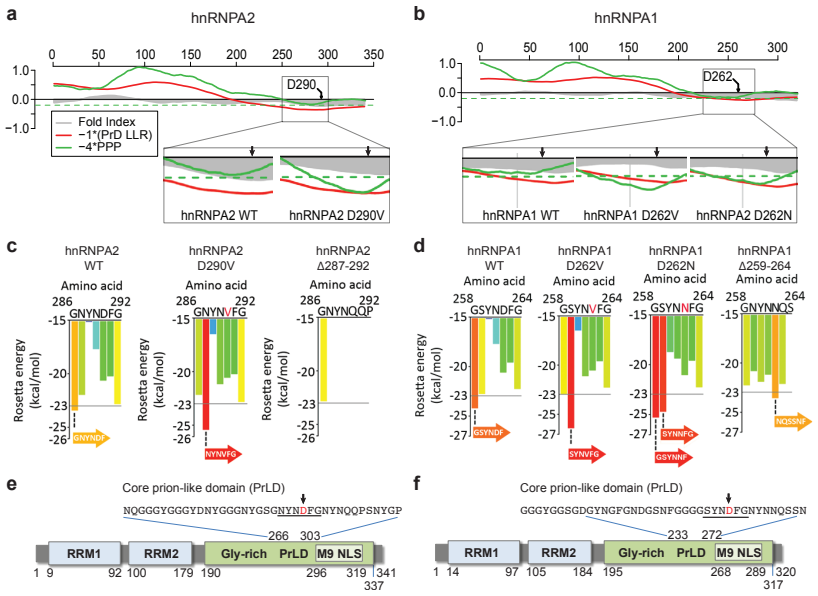

Figure 6. We examined hnRNPA2 and hnRNPA1 with ZipperDB, a structure-based threading algorithm, which scores 6-amino acid segments for their propensity to form 2 self-complementary beta strands termed “steric zippers” that form the spine of amyloid fibrils[4]. Hexapeptides with a Rosetta energy lower than -23 kcal/mol are predicted to form steric zippers, with lower energy predicting higher amyloidogenicity. ZipperDB predicted that the D290V mutation in hnRNPA2 causes a mutant hexapeptide (residues 287-292: NYNVFG) to become highly amyloidogenic (Rosetta energy = -25.5 kcal/mol), whereas the wild-type peptide (NYNDFG) is not (Rosetta energy = -21.9 kcal/mol). Similarly, ZipperDB predicted that the D262V mutation in hnRNPA1 causes a mutant hexapeptide (residues 259-264: SYNVFG) to become highly amyloidogenic (Rosetta energy = -26.4 kcal/mol), whereas the wild-type peptide (SYNDFG) is not (Rosetta energy = -22.8 kcal/mol).

Intriguingly, ZipperDB predicts that the ALS-connected D262N mutation in hnRNPA1 causes two hexapeptides to become more amyloidogenic. First, the hexapeptide comprising residues 258-263 (GSYNNF) becomes more amyloidogenic (Rosetta energy = -25.3 kcal/mol) compared to the wild-type counterpart (GSYNDF), which interestingly also breaches the critical threshold (Rosetta energy = -24.2 kcal/mol). Second, the hexapeptide comprising residues amino acids 259-264 (SYNNFG) also becomes more amyloidogenic (Rosetta energy = -24.7 kcal/mol) compared to the wild-type version (SYNNFG, Rosetta energy = -22.8 kcal/mol). Thus, in all cases the disease-associated mutations introduce potent steric zipper motifs into the PrLD. Importantly, in both hnRNPA1 D262V and hnRNPA2 D290V a mutant hexapeptide is predicted by ZipperDB to have the highest fibrillization propensity in the entire PrLD. For hnRNPA1 D262N, the mutant steric zipper motifs rank second and fourth for fibrillization propensity in the PrLD. The introduction of additional potent steric zipper motifs by the disease-causing mutations in a PrLD is likely to be significant for two reasons. First, introduction of similarly potent steric zipper motifs is sufficient to force fibril formation in model proteins, such as RNase A that would not ordinarily fibrillize[5].

Second, although many (if not all) proteins harbor steric zipper motifs they are usually buried or contorted in protein structures such that they are unable to make the intermolecular contacts necessary for fibril formation[4]. This is not the case in hnRNPA1 and hnRNPA2 as the PrLD is likely to be intrinsically disordered. Thus, the potent steric zipper motifs of mutant hnRNPA1 and hnRNPA2 are available to make intermolecular contacts and drive fibril formation. The hexapeptide 287-292 in hnRNPA2 is critical for spontaneous and seeded fibrillization of full-length WT hnRNPA2 and D290V (Fig. 4e). Likewise, residues 259-264 are essential for spontaneous and seeded fibrillization of WT hnRNPA1, D262V, and D262N (Fig. 4g). The WT versions of these hexapeptides do not fibrillize (Fig. 4a-d). However, the adjacent hexapeptides shifted by one residue towards the N-terminus in WT hnRNPA2 (amino acids 286-291: GNYNDF; Rosetta energy=-23.4kcal/mol) or in WT hnRNPA1 (amino acids 258-263: GSYNDF; Rosetta energy=-24.2kcal/mol), are also predicted to be steric zipper motifs (although not as strongly as the disease-associated mutant hexapeptides). These steric zippers likely drive assembly of WT hnRNPA2 and A1 (Fig. 3c, d). Indeed, deletion of amino acids 259-264 in hnRNPA1 and 287-292 in hnRNPA2 also eliminates these WT steric zipper motifs (Fig. 3c, d) and fibrillization (Fig. 4e, g), which suggests that no other steric zipper motifs in the WT PrLD of hnRNPA2 or A1 are capable of driving fibrillization.

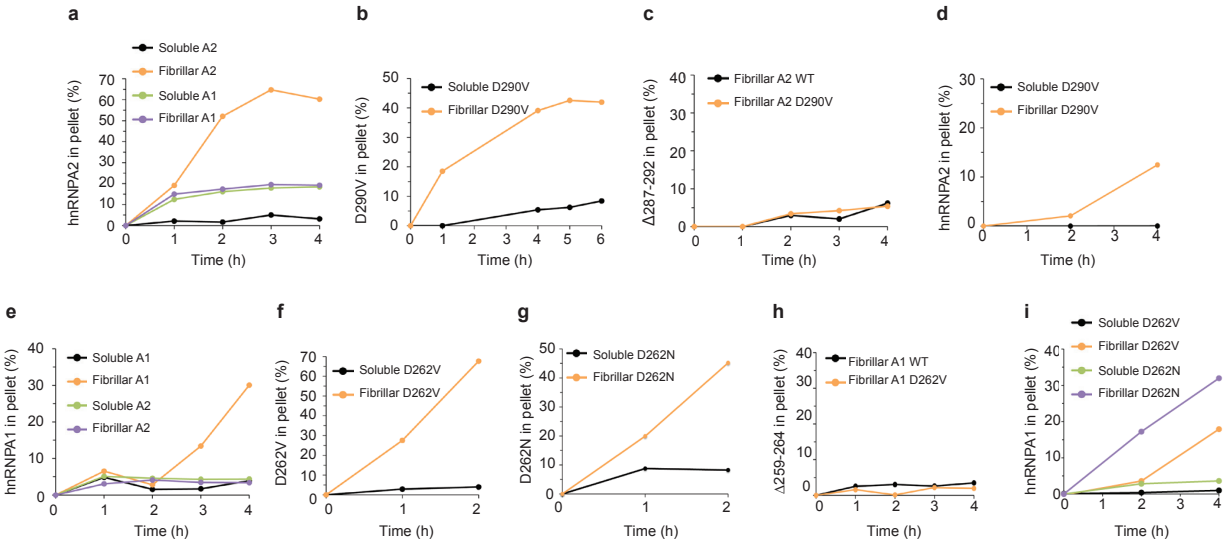

Figure 7. Preformed fibrilar form of mutant proteins can seed their wild type counterpart. **a.** hnRNPA2 (2.5 μM) was incubated for 0-4h at 25°C with agitation (1200 rpm) in the presence of the indicated seed (5% wt/wt) comprised of either soluble hnRNPA2 (black), fibrillar hnRNPA2 (orange), soluble hnRNPA1 (green), or fibrillar hnRNPA1 (purple). At the indicated times, the amount of aggregated hnRNPA2 was determined by sedimentation analysis. A representative data set of several replicates is shown. **b.** hnRNPA2-D290V (2.5 μM) was incubated for 0-6h at 25°C with agitation (1200 rpm) in the presence of the indicated seed (5% wt/wt) comprised of either soluble hnRNPA2-D290V (black) or fibrillar hnRNPA2 D290V (orange). At the indicated times, the amount of aggregated hnRNPA2-D290V was determined by sedimentation analysis. A representative data set of several replicates is shown. **c.** hnRNPA2$^{\Delta 287\text{-}292}$ (5 μM) was incubated for 0-4h at 25°C with agitation (1200 rpm) in the presence of the indicated seed (5% wt/wt) comprised of either fibrillar hnRNPA2 (black) or fibrillar hnRNPA2-D290V (orange). At the indicated times, the amount of aggregated hnRNPA2$^{\Delta 287\text{-}292}$ was determined by sedimentation analysis. A representative data set of several replicates is shown. **d.** hnRNPA2 (5 μM) was incubated for 0-4h at 25°C without agitation in the presence of the indicated seed (10% wt/wt) comprised of either soluble hnRNPA2-D290V (black) or fibrillar hnRNPA2-D290V (orange). At the indicated times, the amount of aggregated hnRNPA2 was determined by sedimentation analysis. A representative data set of several replicates is shown. **e.** hnRNPA1 was incubated for 0-4h at 25°C with agitation in the presence of the indicated soluble (black) or fibrillar (orange) hnRNPA1 seed (5% wt/wt), or soluble (green) or fibrillar (purple) hnRNPA2 seed (5% wt/wt). At various times, the amount of aggregated hnRNPA1 was determined. A representative dataset is shown**. f.** hnRNPA1-D262V was incubated for 0-2h at 25°C with agitation in the presence of the indicated soluble (black) or fibrillar (orange) hnRNPA1-D262V seed (5% wt/wt). At various times, the amount of aggregated hnRNPA1 D262V was determined. A representative dataset is shown. **g.** hnRNPA1-D262N was incubated for 0-2h at 25°C with agitation in the presence of the indicated soluble (black) or fibrillar (orange) hnRNPA1-D262N seed (5% wt/wt). At various times, the

amount of aggregated hnRNPA1-D262N was determined. A representative dataset is shown. **h.** hnRNPA1$^{\Delta 259\text{-}264}$ was incubated for 0-4h at 25°C with agitation in the presence of the indicated fibrillar hnRNPA1 (black) or fibrillar hnRNPA1-D262V (orange) seed (5% wt/wt). At various times, the amount of aggregated hnRNPA1$^{\Delta 259\text{-}264}$ was determined. A representative dataset is shown. **i.** hnRNPA1 was incubated for 0-4h at 25°C without agitation in the presence of soluble hnRNPA1 D262V (black), soluble hnRNPA1-D262N (green), sonicated fibrillar hnRNPA1 D262V (orange), or sonicated fibrillar hnRNPA1-D262N (purple) seed (5% wt/wt). At various times, the amount of aggregated hnRNPA1 was determined. A representative dataset is shown.

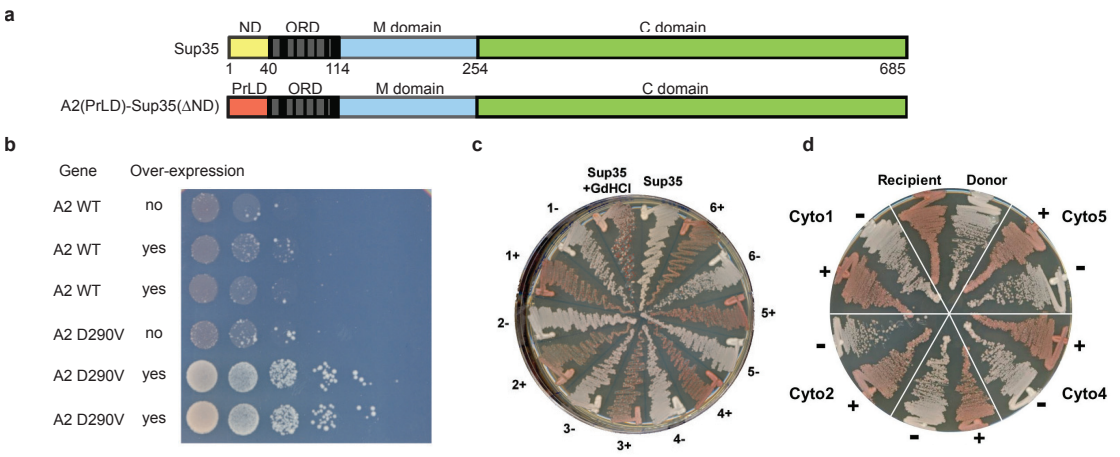

Figure 8. To determine whether the PrLD of hnRNPA2/B1 could support prion nucleation activity in yeast, we replaced the Sup35 nucleation domain (residues 3-40) with the wild-type or mutant hnRNPA2 core PrLD (residues 261-303), and expressed these fusions (referred to as A2-Sup35) as the sole copy of Sup35 in the cell (**a**). Prion formation was detected by monitoring nonsense suppression of the *ade2-1* allele. *ade2-1* mutants are unable to grow in the absence of adenine and grow red on limiting adenine. [*PSI*$^+$] increases stop codon read-through, allowing *ade2-1* mutants to grow in the absence of adenine and grow white on limiting adenine. Strains expressing these fusions as the sole copy of Sup35 were transformed with either an empty vector (pKT24) or pKT24 modified to express the prion domain from the matching hnRNPA2/B1-Sup35 fusion from the GAL1 promoter. Cells were grown in galactose/raffinose dropout medium, and plated onto medium lacking adenine to select for prion formation. When cells expressing the wild-type and D290V A2-Sup35 fusions were plated on medium lacking adenine, rare colonies were formed, consistent with prion formation. One hallmark of prions is that the frequency of prion formation should be dependent on the expression level of the prion protein. Transient over-expression of the wild-type A2-Sup35 chimeric prion domain did not substantially increase Ade$^+$ colony formation (**b**). By contrast over-expression of the D290V A2-Sup35 prion domain substantially increased Ade$^+$ colony formation (**b**), suggesting that the D290V fusion is forming prions. To further demonstrate that the Ade$^+$ phenotype observed for the D290V fusion was due to a prion formation, Ade$^+$ isolates were tested for curability and stability of the Ade$^+$ phenotype. Six independent Ade+ isolates formed by strains expressing the D290V-Sup35 fusion were grown on YPD (-) and YPD with 4 mM guanidine HCl (+), and then re-streaked on YPD to test for loss of the Ade+ phenotype. An identically treated [PSI+] strain expressing wild type Sup35 is included as a control. Almost all Ade$^+$ isolates stably maintained the Ade$^+$ phenotype when grown on non-selective medium, but lost the Ade$^+$ phenotype when grown on medium containing low concentrations of guanidine HCl (**c**). Guanidine HCl cures almost all yeast prions by inhibiting Hsp104[6-8], a chaperone required for prion propagation[9]. By contrast, none of the Ade$^+$ isolates from the wild-type fusion were both stable and curable (**c**). Furthermore, the Ade$^+$ phenotype in the mutants was transferable by cytoduction (**d**), a method that transfers cytoplasmic

elements, but not nuclear genes[10]. Ade+ isolates from cells expressing the D290V A2-Sup35 fusion were used as donors for cytoduction reactions. Recipient cells also expressed the D290V A2-Sup35 fusion as the sole copy of Sup35. Donor and recipient cells were streak onto YPD, along with individual cytoductants before (-) and after (+) treatment with guanidine HCl. These results demonstrate that the Ade^{+} phenotype is the result of prion formation. Collectively, these experiments show that the core D290V PrLD can substitute for the Sup35 nucleation domain in supporting prion formation, and that the D290V mutation specifically promotes the nucleation activity.

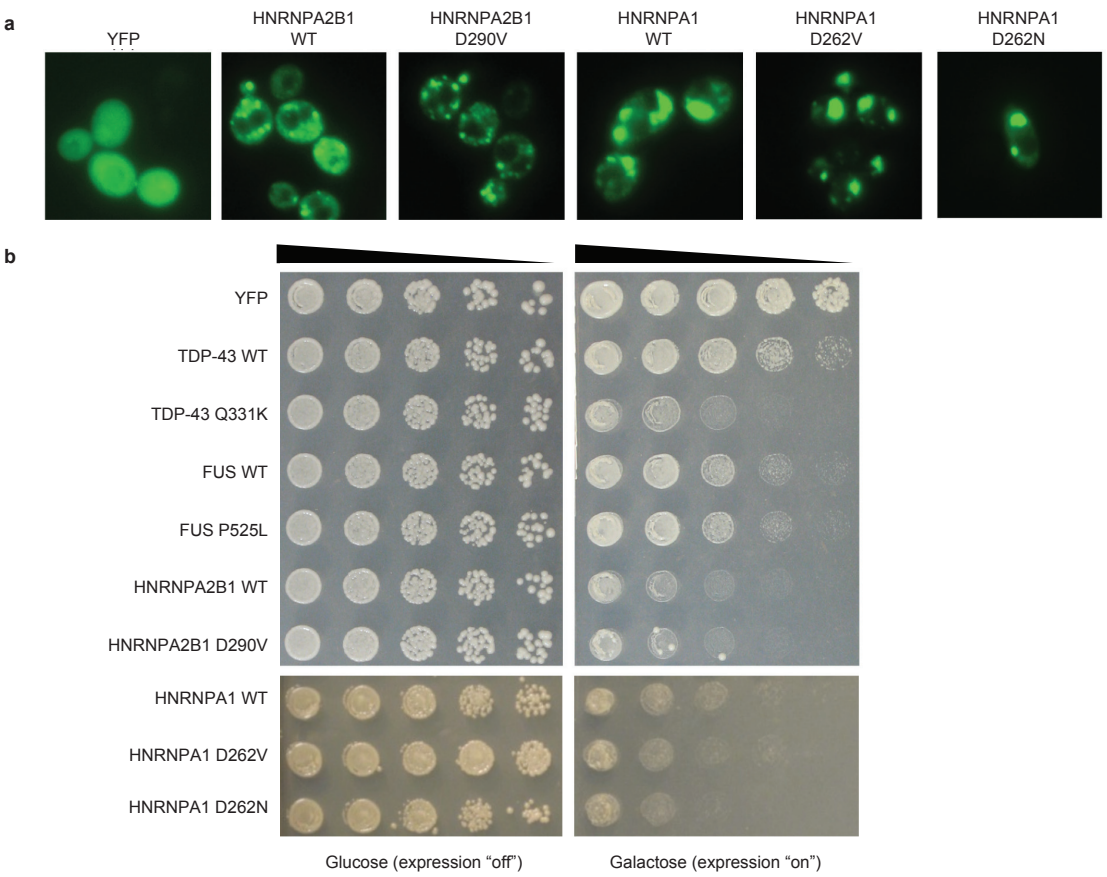

Figure 9. HnRNPA2 and hnRNPA1 aggregate in yeast and are toxic. **a.** Yeast cells expressing YFP alone or YFP-tagged WT and mutant human RBPs HNRNPA2B1 and HNRNPA1. YFP was diffusely localized throughout the cytosol and nucleus, whereas wild-type and mutant hnRNPA2 and hnRNPA1 formed multiple cytoplasmic foci when expressed in yeast. The mutant forms of hnRNPA2 and hnRNPA1 formed similar numbers of cytoplasmic foci as WT. **b.** HNRNPA2 and HNRNPA1 are toxic when expressed in yeast. Yeast spotting assays comparing toxicity of TDP-43, FUS, hnRNPA2, and hnRNPA1. WT TDP-43 is toxic when expressed in yeast and an ALS-linked mutation (Q331K) increases toxicity. WT FUS is also toxic when expressed in yeast and ALS-linked mutations (e.g. P525L) do not increase toxicity. WT HNRNPA2 and HNRNPA1 are very toxic when expressed in yeast and the MSP-associated mutant forms do not enhance toxicity in this assay. Because of the galactose-inducible promoter, expression of these RBPs is repressed when cells are grown in the presence of glucose (left panel, expression "off") and induced when grown in the presence of galactose (right panel, FUS expression "on").

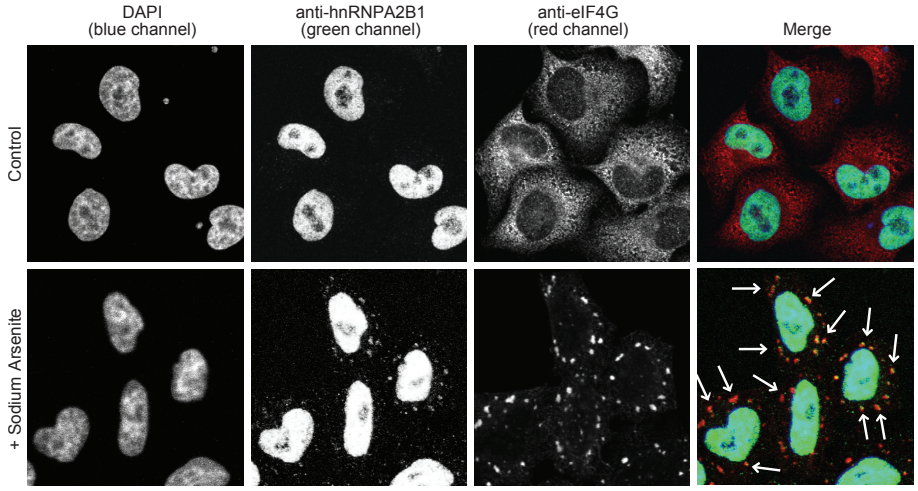

Figure 10. Endogenous hnRNPA2B1 is recruited to SGs following treatment with arsenite. HeLa cells were treated with 0.5 mM sodium arsenite for 1h and stained with anti-Flag (green), anti-eIF4G (red), and DAPI (blue).

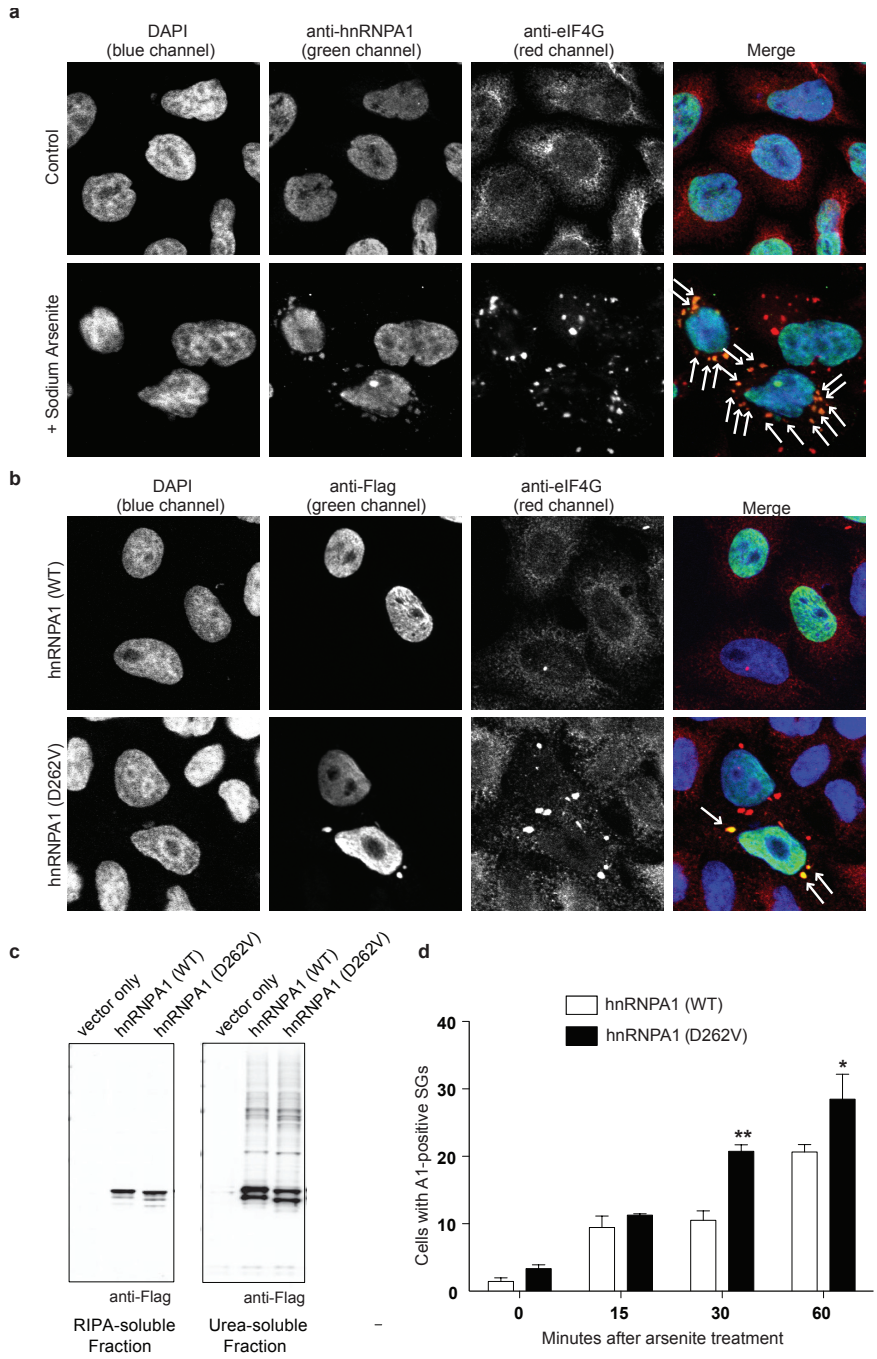

Figure 11. hnRNPA1 is recruited to SGs and this is augmented by disease-causing mutation. **a.** Endogenous hnRNPA1 was recruited to SGs following treatment with arsenite. **b.** HeLa cells were transfected with either the Flag-wild-type or Flag-D262V mutant form of hnRNPA1 and stained with anti-Flag (green), anti-eIF4G (red), and DAPI (blue). Arrows indicate hnRNPA1- and eIF4G-positive SGs. **c.** Immunoblot of hnRNPA1 in the RIPA-soluble and RIPA-insoluble (Urea-soluble) fractions from transfected HeLa cells. **d.** Quantification of the number of cells displaying hnRNPA1–positive SGs. The

percentage of cells displaying hnRNPA1-positive SGs at indicated time points following treatment with arsenite cells are plotted. Data represent mean ± SEM of at least 3 independent experiments (* $P<0.05$, ** $P<0.01$). P values are compared with wild type control.

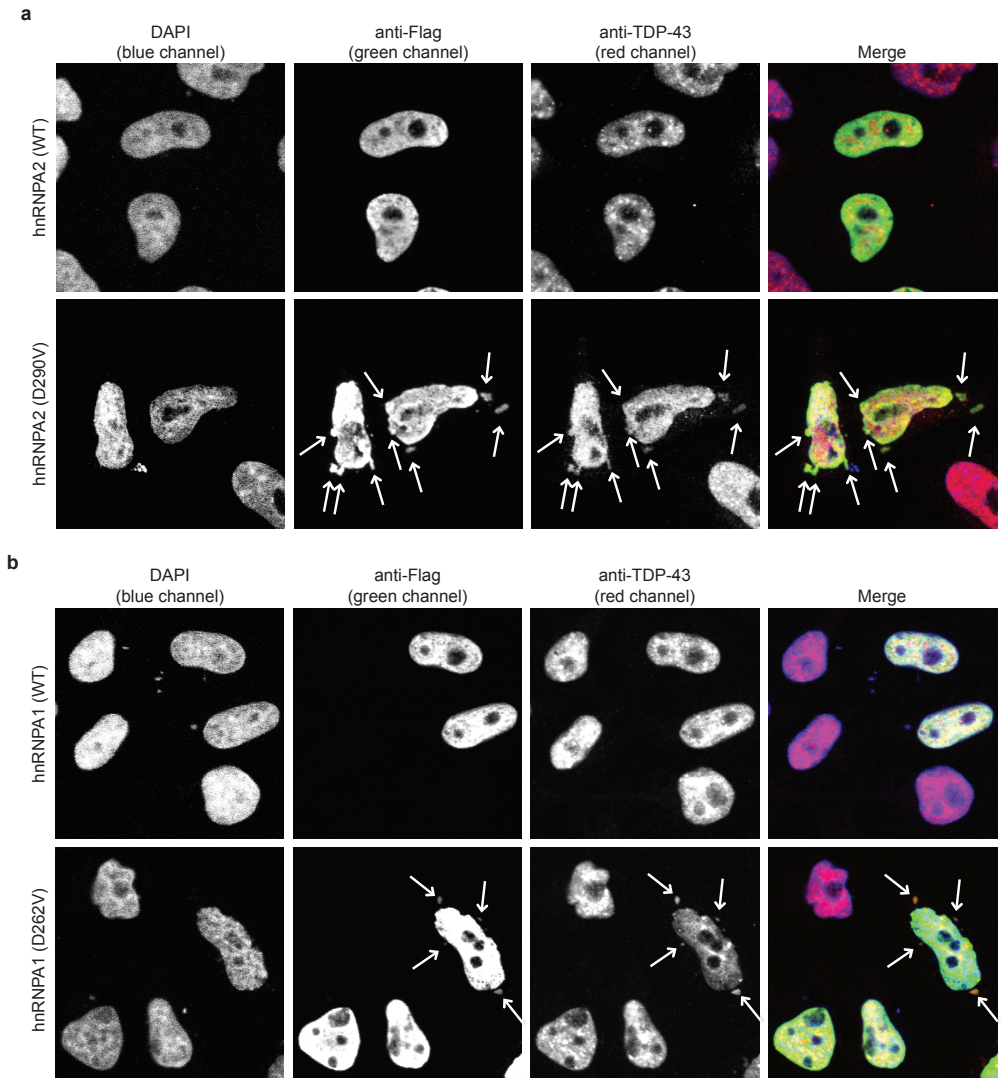

Figure 12. Colocalization of hnRNPA2 and hnRNPA1 with TDP-43 in SGs. **a.** HeLa cells were transfected with either Flag-wild-type or Flag-D290V mutant form of hnRNPA2 and stained with anti-Flag (green), anti-TDP-43 (red), and DAPI (blue). Arrows indicate hnRNPA2 and TDP-43 positive SGs. **b.** HeLa cells were transfected with either Flag-wild-type or Flag-D262V mutant form of hnRNPA1 and experiments are performed as in **a.**

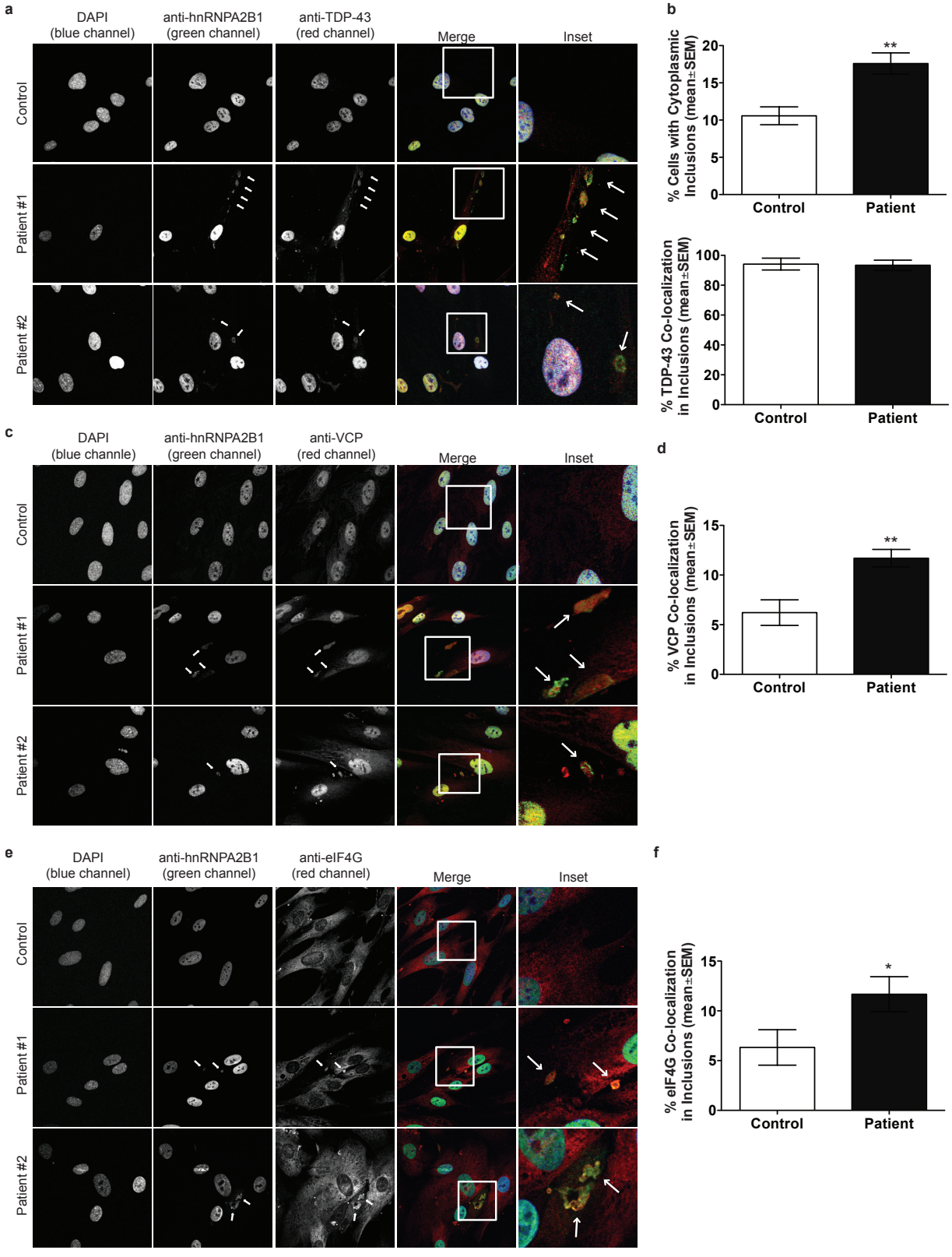
a
DAPI (blue channel)
anti-hnRNPA2B1 (green channel)
anti-TDP-43 (red channel)
Merge
Inset
Control
Patient #1
Patient #2
b
% Cells with Cytoplasmic Inclusions (mean±SEM)
20
15
10
5
0
**
Control
Patient
% TDP-43 Co-localization in Inclusions (mean±SEM)
100
80
60
40
20
0
Control
Patient
c
DAPI (blue channle)
anti-hnRNPA2B1 (green channel)
anti-VCP (red channel)
Merge
Inset
Control
Patient #1
Patient #2
d
% VCP Co-localization in Inclusions (mean±SEM)
15
10
5
0
**
Control
Patient
e
DAPI (blue channel)
anti-hnRNPA2B1 (green channel)
anti-eIF4G (red channel)
Merge
Inset
Control
Patient #1
Patient #2
f
% eIF4G Co-localization in Inclusions (mean±SEM)
15
10
5
0
*
Control
Patient

Figure 13. hnRNPA2B1 localization in control and patients fibroblasts. **a.** Control and patients fibroblasts were stained with anti-hnRNPA2B1 (green), anti-TDP-43 (red), and DAPI (blue). Arrows indicate cytoplasmic granules displaying colocalization of hnRNPA2B1 with TDP-43. **b.** Percentage of cells displaying hnRNPA2B1-positive cytoplasmic inclusions (upper panel), and percentage of cells displaying hnRNPA2B1 and TDP-43 colocalization in inclusions (number of cells with hnRNPA2B1+, TDP-43+ in inclusions / number of cells with hnRNPA2/B1+ in inclusions, lower panel) in control and patients fibroblasts. **c.** Control and patient fibroblasts were stained with anti-hnRNPA2B1 (green), anti-VCP (red), and DAPI (blue). Arrows indicate cytoplasmic granules displaying colocalization of hnRNPA2 with VCP. **d.** Percentage of cells displaying hnRNPA2B1 and VCP colocalization in inclusions (number of cells with hnRNPA2B1+, VCP+ in inclusions / total number of cells) in control and patients fibroblasts. **e.** Control and patients fibroblasts were stained with anti-hnRNPA2B1 (green), anti-eIF4G (red), and DAPI (blue). Arrows indicate cytoplasmic granules displaying colocalization of hnRNPA2 with eIF4G. **f.** Percentage of cells displaying hnRNPA2B1 and eIF4G colocalization in inclusions (number of cells with hnRNPA2B1+, eIF4G+ in inclusions / total number of cells) in control and patients fibroblasts. Data represent mean ± SEM of at least 3 independent experiments (* $P<0.05$, ** $P<0.01$). P values are compared with wild type control.

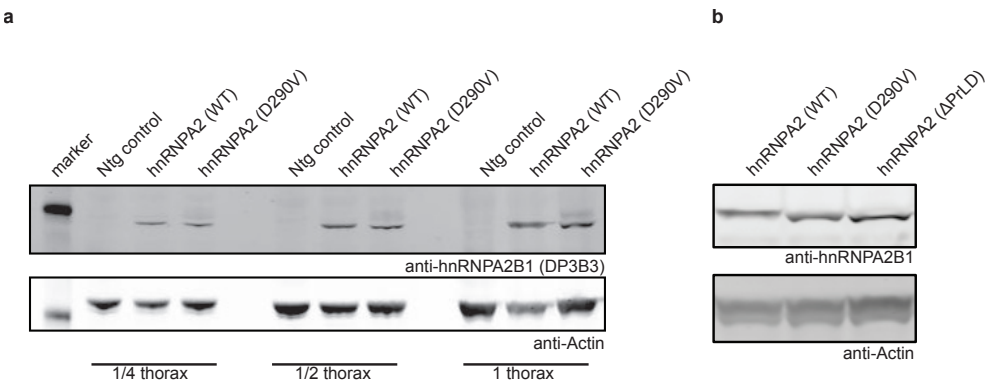

Figure 14. Comparable levels of hnRNPA2 expression transgenic flies. **a-b.** Thoraces of adult flies were processed for Western blot analysis with an antibody against hnRNPA2/B1. Actin was blotted as a loading control.

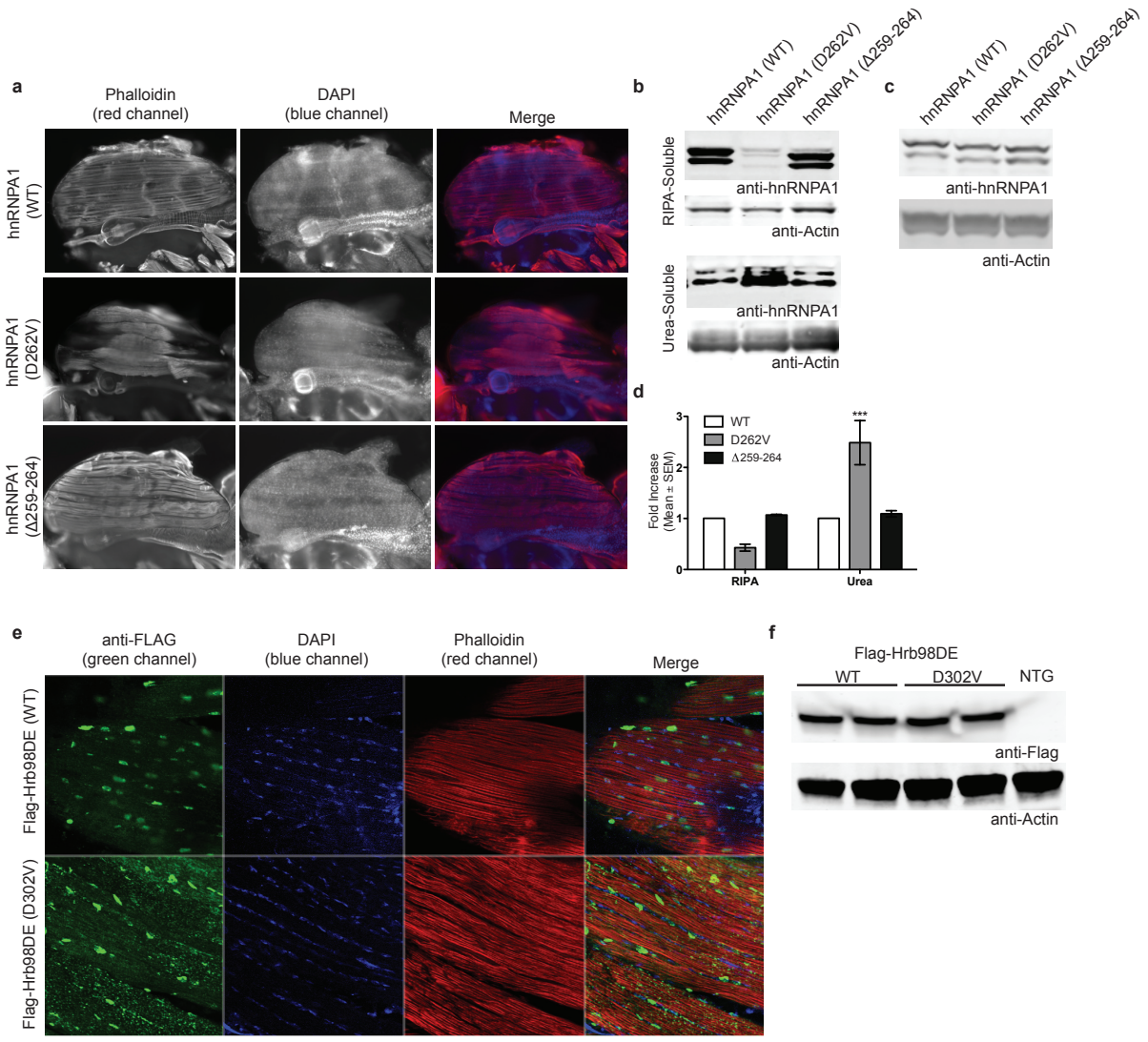

Figure 15. Mutant hnRNPA1 and Hrb98DE accumulate in pathological inclusions in Drosophila. **a.** Adult flies were dissected to expose the dorsal longitudinal indirect fly muscle (DLM) and stained with Texas Red-phalloidin (red), and DAPI (blue). **b.** Thoraces of adult flies were dissected. Sequential extractions were performed to examine the solubility profile of hnRNPA1**. c.** Thoraces of adult flies were processed for Western blot analysis with an antibody against hnRNPA1. **d.** Quantification of the blot shown in **b**. *** $p < 0.001$. P values are compared with wild type (WT). **e**. DLM of Adult flies were dissected and stained with anti-Flag (green), Texas Red-phalloidin (red), and DAPI (blue). **f.** Thoraces of adult flies were processed for Western blot analysis with an antibody against Flag.

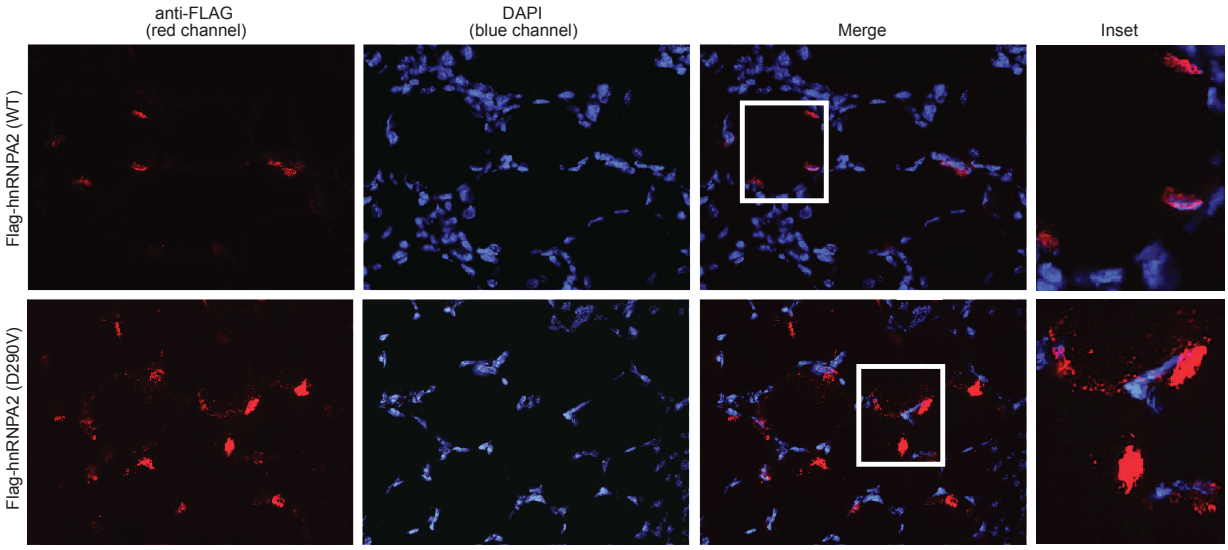

Figure 16. Mutant hnRNPA2 accumulates in pathological inclusions in mouse muscle. Mouse tibialis anterior was electroporated with plasmid expressing either wild-type Flag-hnRNPA2 or mutant Flag-hnRNP (D290V). After a 7-day recovery, wild-type hnRNPA2 was found to localize exclusively to myonuclei whereas mutant hnRNPA2 (D290V) also accumulated extensively in sarcoplasmic aggregates.

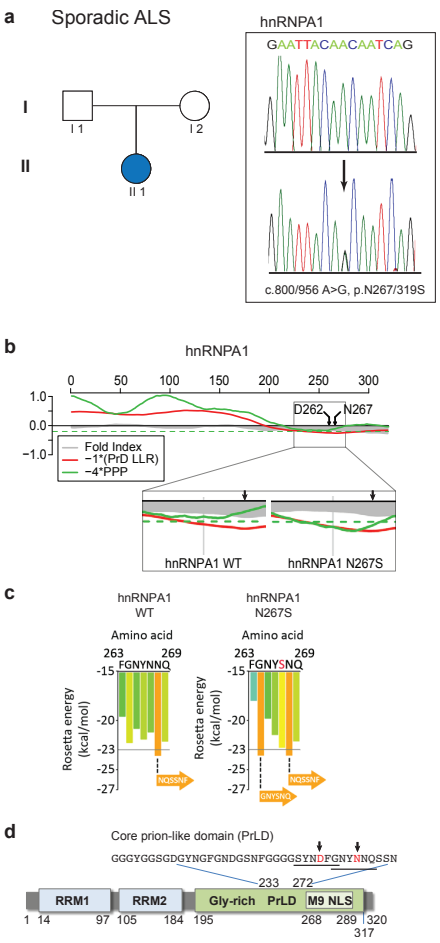

Figure 17. The disease-causing mutation impact a PrLD in hnRNPA1 in sporadic ALS. **a.** We screened 305 sporadic ALS cases and identified a nonsynonymous variant in hnRNPA1 (c.800/956A>G, p.N267/319S) in one classic, late-onset case in which mutations in known ALS genes had been excluded (c9orf72, SOD1, TARDBP, FUS and PNF1). **b.** PrLD prediction for hnRNPA1. The panel shows the FoldIndex prediction of an extended intrinsically unfolded region (grey curve less than zero) in the C-terminus of hnRNPA1. Part of this region was also predicted to be prion-like according to the algorithm of Alberti et al. (red curve less than zero), and narrowly missed the cutoff for the prion propensity algorithm of Toombs et al. (green curve below the dashed green line). All curves represent averages of 41 consecutive windows of 41 amino acids, corresponding to the criteria of Toombs et al. The N267S mutation in hnRNPA1 was predicted to make this region more prionogenic, with a core PrLD that now satisfied all 3 conditions. **c.** ZipperDB detected a 6-amino-acid stretch within the core PrLD for which the N267S mutation increased the predicted amyloid fibril–forming potential beyond the Rosetta threshold. **d.** Domain architecture of hnRNPA1 shows two RNA-recognition motifs, RRM1 and 2, a C-terminal glycine-rich domain, and an M9 nuclear localization signal. The predicted prion-like domain is within the C-terminal glycine-rich domain.

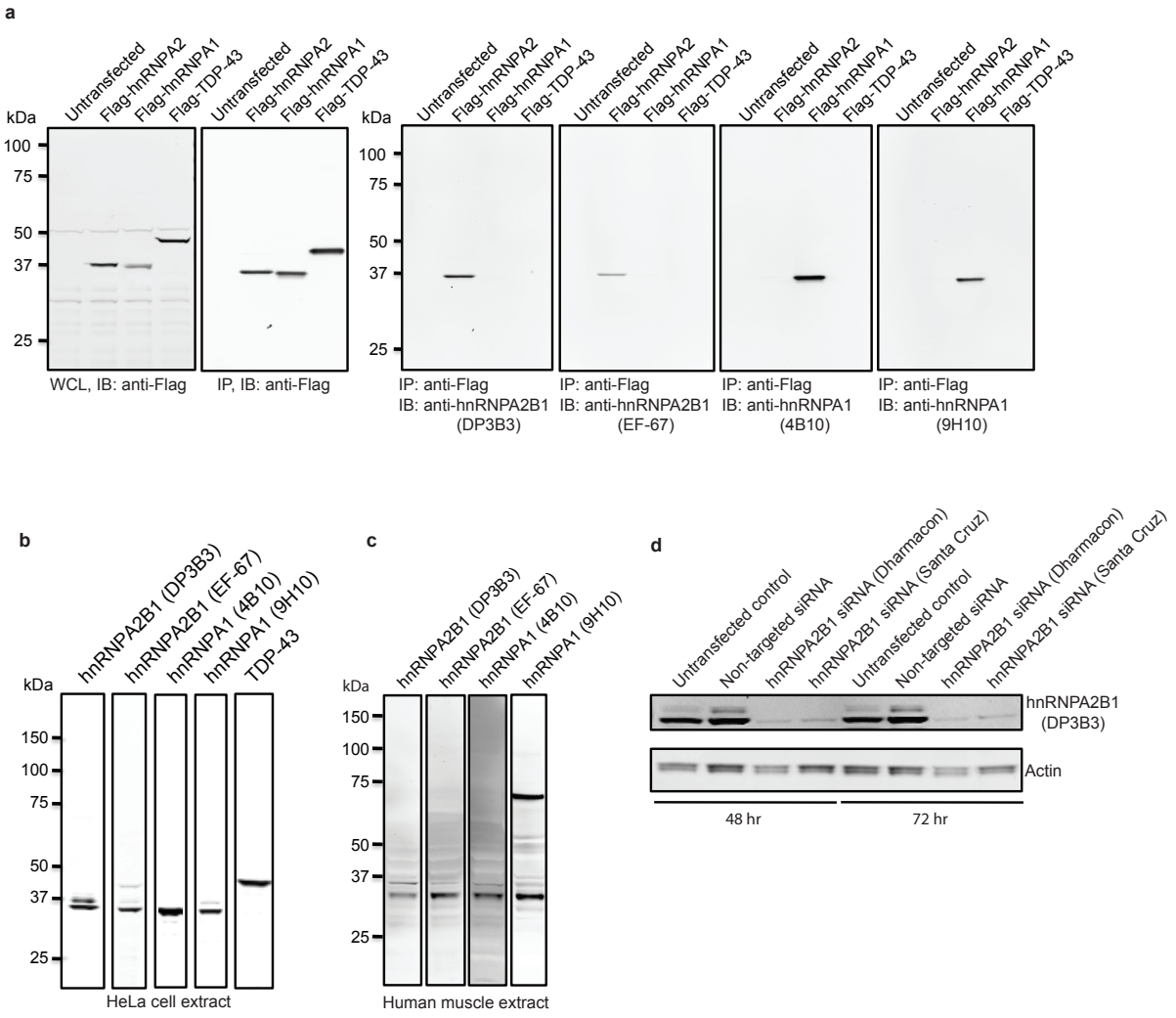

Figure 18. Validation of antibodies used in the experiments. **a.** HeLa cells were transfected with Flag-hnRNPA2, Flag-hnRNPA1 or Flag-TDP-43 as indicated. Immunoprecipitation (IP) was performed with anti-Flag antibody and immunoblotting (IB) was performed with antibodies indicated. **b.** HeLa cell lysates were immunoblotted with antibodies indicated. **c.** Human muscle extract was immunoblotted with antibodies indicated. **d.** HeLa cells were transfected with hnRNPA2B1 specific siRNA. Two and three days post transfection, cell lysates were immunoblotted with hnRNPA2B1 (DP3B3) antibody.

References

1 Waggoner, B. *et al.* Heterogeneity in familial dominant Paget disease of bone and muscular dystrophy. *Am J Med Genet* 108, 187-191, (2002).

2 Ritson, G. P. et al. TDP-43 mediates degeneration in a novel Drosophila model of disease caused by mutations in VCP/p97. J Neurosci 30, 7729-7739, (2010).

3 Couthouis, J. *et al.* A yeast functional screen predicts new candidate ALS disease genes. *Proc Natl Acad Sci U S A* 108, 20881-20890, (2011).

4 Goldschmidt, L., Teng, P. K., Riek, R. & Eisenberg, D. Identifying the amylome, proteins capable of forming amyloid-like fibrils. *Proc Natl Acad Sci U S A* 107, 3487-3492, (2010).

5 Teng, P. K. & Eisenberg, D. Short protein segments can drive a non-fibrillizing protein into the amyloid state. *Protein Eng Des Sel* 22, 531-536, (2009).

6 Ferreira, P. C., Ness, F., Edwards, S. R., Cox, B. S. & Tuite, M. F. The elimination of the yeast [PSI+] prion by guanidine hydrochloride is the result of Hsp104 inactivation. *Mol Microbiol* 40, 1357-1369, (2001).

7 Jung, G. & Masison, D. C. Guanidine hydrochloride inhibits Hsp104 activity in vivo: a possible explanation for its effect in curing yeast prions. *Curr Microbiol* 43, 7-10, (2001).

8 Tuite, M. F., Mundy, C. R. & Cox, B. S. Agents that cause a high frequency of genetic change from [psi+] to [psi-] in Saccharomyces cerevisiae. *Genetics* 98, 691-711, (1981).

9 Chernoff, Y. O., Lindquist, S. L., Ono, B., Inge-Vechtomov, S. G. & Liebman, S. W. Role of the chaperone protein Hsp104 in propagation of the yeast prion-like factor [psi+]. *Science* 268, 880-884, (1995).

10 Conde, J. & Fink, G. R. A mutant of Saccharomyces cerevisiae defective for nuclear fusion. *Proc Natl Acad Sci U S A* 73, 3651-3655, (1976).